

# Direct Gravure Printing of Silicon Nanowires Using Entropic Attraction Forces

Jungmok Seo, Hyonik Lee, Seulah Lee, Tae Il Lee, Jae-Min Myoung, and Taeyoon Lee\*

*The development of a method for large-scale printing of nanowire (NW) arrays onto a desired substrate is crucial for fabricating high-performance NW-based electronics. Here, the alignment of highly ordered and dense silicon (Si) NW arrays at anisotropically etched micro-engraved structures is demonstrated using a simple evaporation process. During evaporation, entropic attraction combined with the internal flow of the NW solution induced the alignment of NWs at the corners of pre-defined structures, and the assembly characteristics of the NWs were highly dependent on the polarity of the NW solutions. After complete evaporation, the aligned NW arrays are subsequently transferred onto a flexible substrate with 95% selectivity using a direct gravure printing technique. As a proof-of-concept, flexible back-gated NW field-effect transistors (FETs) are fabricated. The fabricated FETs have an effective hole mobility of  $17.1 \text{ cm}^2 \cdot \text{V}^{-1} \cdot \text{s}^{-1}$  and an on/off ratio of  $\sim 2.6 \times 10^5$ .*

## 1. Introduction

Over the past few decades, 1D nanostructures such as carbon nanotubes (CNTs), nanorods, and nanowires (NWs) have been actively studied as promising potential building blocks for a wide range of novel electronic devices and sensors.<sup>[1–12]</sup> In particular, these 1D nanostructures are suited for application in flexible electronics because of their particular mechanical flexibility and electrical properties.<sup>[13–18]</sup> However, an important technical issue that has to be addressed to fabricate 1D nanostructure-based devices commercially is the

placement of NWs in the desired patterns during large-scale assembly.

Several methods that exploit a diverse set of external forces and internal interactions to pattern NWs and nanoparticles have been reported, including the Langmuir–Blodgett technique,<sup>[19]</sup> electronic/magnetic field-assisted assembly,<sup>[20,21]</sup> microfluidic assembly,<sup>[22,23]</sup> capillary and convective force-driven assembly,<sup>[24–27]</sup> blown-bubble film technique,<sup>[28]</sup> and self-assembled monolayer (SAM)-assisted microcontact printing.<sup>[29–31]</sup> Because NWs are commonly suspended in a liquid solution during the alignment process, the aforementioned techniques require a solvent evaporation step. Thus, an understanding of how suspended NWs move in solvent, near the solvent–substrate interface, and at the contact line during evaporation is critical to develop a solution-based NW alignment method.

The motion of nanoparticles suspended in solution during evaporation was investigated by Deegan and colleagues.<sup>[32]</sup> They reported that during evaporation of a nanoparticle-containing solution, the outward capillary force of the solvent caused the nanoparticles to move toward the solvent–substrate contact line to compensate for the loss of solvent at the periphery of the solution. Recently, Huang et al.<sup>[33]</sup> demonstrated vertically aligned Ag NW arrays using this outward capillary flow combined with a programmed slip-stick motion at the solution–substrate contact line by controlling

J. Seo, H. Lee, S. Lee, Prof. T. Lee  
Nanobio Device Laboratory  
School of Electrical and Electronic Engineering  
Yonsei University  
134 Shinchon-Dong, Seodaemun-Gu  
Seoul 120-749, Republic of Korea  
E-mail: taeyoon.lee@yonsei.ac.kr

T. I. Lee, J.-M. Myoung  
Information and Electronic Materials Research Laboratory  
Department of Materials Science and Engineering  
Yonsei University  
134 Shinchon-dong, Seodaemun-gu  
Seoul 120-749, Republic of Korea

DOI: 10.1002/sml.201102367



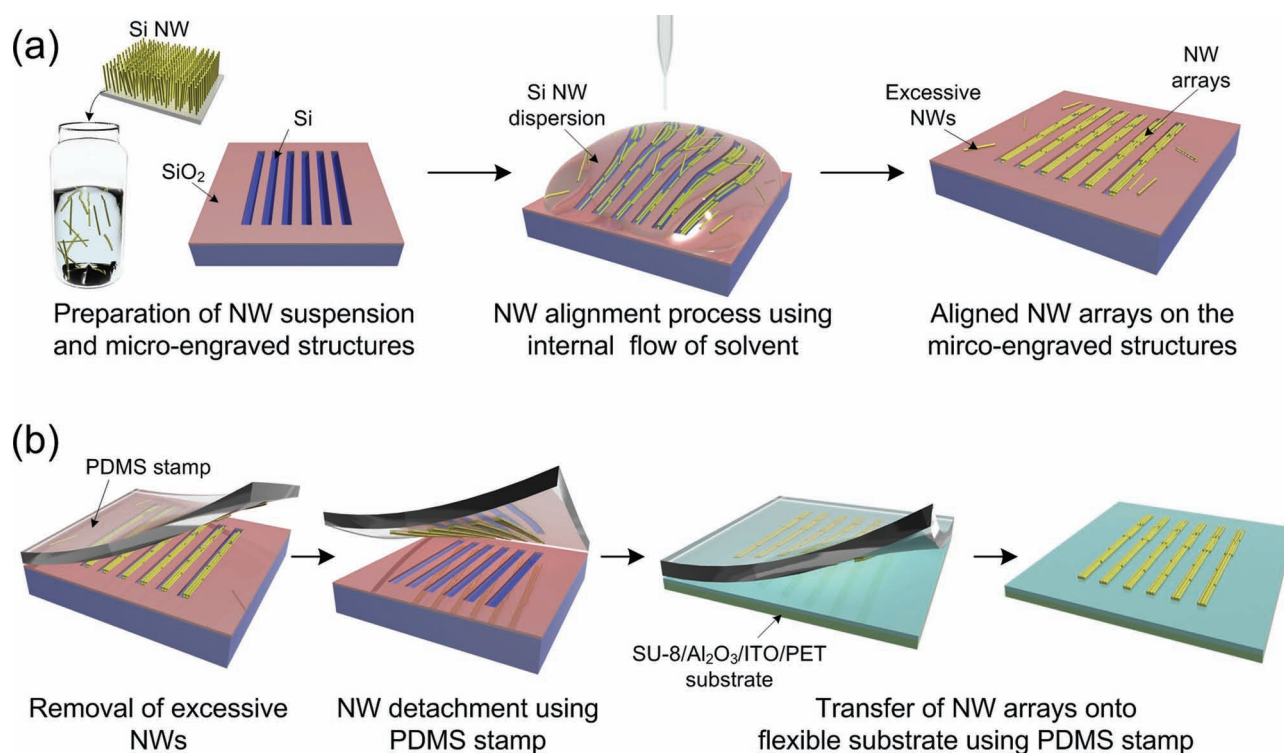


**Figure 1.** Fabrication process used to align NWs and transfer Si NW arrays to a flexible substrate. a) Illustration of the alignment of Si NWs in a micro-engraved substrate. b) Schematic diagram of the direct gravure printing technique used to fabricate highly ordered NW arrays on a flexible substrate.

the pulling speed of a substrate dipped vertically in the solution. Furthermore, Li et al.<sup>[34]</sup> proposed a simple method to align highly dense  $\text{Na}_{0.44}\text{MnO}_2$  NW networks by an addition of a graphene oxide (GO) nanosheet to a NW-containing solution. The aligned NWs were parallel to the contact line of the liquid/hydrophilic-substrate as a direct result of the modified surface properties of the NWs: GO-adsorbed NWs were enriched at the surface between the air and solution, enabling effective alignment of the NWs at the contact line. Although the techniques described above allow the simple arrangement of NWs, the NWs can only be aligned at the contact line between the solvent and the substrate. Moreover, because the substrates are submerged and then pulled out in a specific manner, the aligned NWs can only adopt an orientation parallel to the contact line, limiting the types of possible NW array patterns.

In this report, we propose a novel method of aligning Si NWs into predefined patterns that we call direct gravure printing. Our results show that our NW alignment technique, which exploits the internal hydrodynamic flow of the NW solution and entropic force fields, can be used to align NW arrays in any pattern desired. During evaporation of the NW solution, the NWs move spontaneously into micro-engraved structures because of the activated internal hydrodynamic flow of the NW solution. The entropic attraction between the NWs and engraved structure then results in the NWs being captured at the corners of the structures. Notably, we found that the movements of the NWs were significantly affected by the polarity of the solvents: in polar solutions,

the outward direction of the flow field allowed the NWs to move freely, resulting in selectively assembled NW arrays; in contrast, in nonpolar solutions, the movements of the NWs were restricted because of the static flow field, leading to a random distribution of NWs on the substrate. The aligned NW arrays were selectively transferred to a flexible substrate by the direct gravure printing technique, using functionally specified flat polydimethylsiloxane (PDMS) stamps as follows. First, redundant NWs located at undesirable positions were removed using a rigid PDMS stamp with low adhesion; subsequently, the NW arrays aligned at the micro-engraved structures were detached using a soft PDMS stamp with high adhesion, and then transferred to the desired substrate. We demonstrated large-scale Si NW field-effect transistors (FETs) on a flexible substrate as a proof-of-concept.

## 2. Results and Discussion

**Figure 1** schematically illustrates the procedures used to align NWs and transfer Si NW arrays onto a flexible substrate. Two main steps are involved: the alignment of Si NWs on the micro-engraved substrate (Figure 1a), followed by the direct gravure printing of NW arrays onto the flexible substrate (Figure 1b). The Si NWs were fabricated using an aqueous electroless etching (AEE) method.<sup>[35]</sup> Then, they were cut into the various solutions and well dispersed. The NW suspension was dropped and evaporated on the micro-engraved substrate, which was covered with a  $\text{SiO}_2$  layer except for

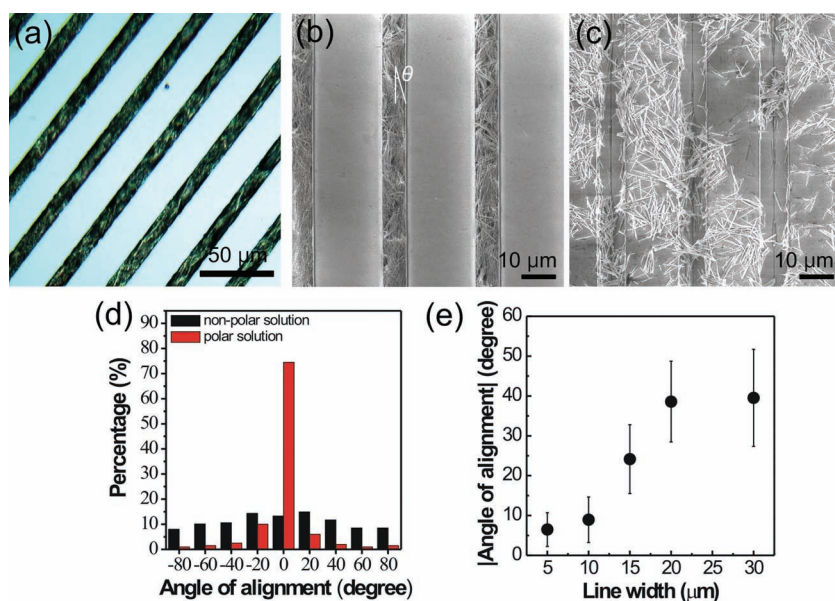


**Figure 2.** Selectively aligned Si NW arrays at the micro-engraved structures. a) Optical image and b) its corresponding SEM image, using a polar solvent (DI water). c) SEM image of randomly distributed Si NWs deposited on the substrate using a nonpolar solvent (chloroform). d) Angular distribution of Si NWs assembled onto line patterned structures. The angle  $\theta$  was measured relative to a reference angle of zero for NWs parallel to the line direction. e) The measured values of deviation angles ( $|\theta|$ ) for various line widths of the line-patterned micro-engraved structures.

the engraved pattern regions. The NWs were well aligned after complete evaporation of the droplet of NW solution; the physics behind this will be discussed in detail later in the manuscript. For direct gravure printing of NW arrays onto the flexible substrate, excess NWs located on the substrate (not in the micro-groove structures) were removed. A flat elastomeric PDMS with high rigidity and low adhesive strength was used to make conformal contact with the substrate, after which the PDMS was carefully peeled off. More than 80% of the redundant NWs located at undesirable positions were removed by this simple correction process, and the number of remaining redundant NWs was minimized by repeating this step. Then, using a softer PDMS with high adhesive strength, the NW arrays located in the micro-engraved structures were successfully separated without affecting their alignment. Finally, the detached Si NW arrays on PDMS were transferred to a flexible  $\text{Al}_2\text{O}_3/\text{ITO}/\text{PET}$  (where ITO is indium tin oxide and PET is poly(ethylene terephthalate)) substrate covered with an epoxy bonding layer with maintaining their original shapes of assembled NW arrays (see Figure S1 in the Supporting Information (SI)).

**Figure 2a** and **b** are typical optical and scanning electron microscopy (SEM) images of the assembled Si NW arrays on a 10- $\mu\text{m}$ -wide line-patterned micro-engraved substrate, obtained using a polar NW solution (de-ionized (DI) water), and **Figure 2c** shows the SEM image of the same using a non-polar NW solution (chloroform). Interestingly, the assembly characteristics of Si NWs were strongly dependent on the polarity of the NW solutions. NWs were selectively assembled and well-aligned inside the line-patterned micro-engraved structures when polar solutions were evaporated. In contrast,

NWs dispersed in nonpolar solutions were rarely assembled in patterns. The assembly selectivity of NWs, which we defined as the percentage of NWs located at the micro-engraved regions, was  $\sim 95\%$  for DI water and  $\sim 32\%$  for chloroform. We observed analogous assembly behavior for various other polar NW solutions (isopropyl alcohol, methyl alcohol, and acetone); among these polar solutions, DI water showed the highest assembly selectivity. Regardless of the nonpolar solution used (toluene, methylene chloride), NWs assembled in a random pattern. We examined the degree of NW alignment according to the polarity of the solutions (**Figure 2d**) by measuring the deviation angle of the aligned NWs with respect to the direction of the line pattern indicated by  $\theta$  in **Figure 2a**. More than  $\sim 73\%$  of NWs were well aligned within  $|\theta| < 10^\circ$  for polar NW solutions, whereas the NWs were randomly oriented in nonpolar NW solutions. In a polar solution, the degree of NW alignments could be affected by the widths of the line-patterned micro-engraved structures. **Figure 2e** exhibits the measured deviation angles ( $|\theta|$ ) of aligned NWs with

varying the line width of the micro-engraved structures from 5 to 30  $\mu\text{m}$ . As shown in **Figure 2e**, the absolute values and the uncertainties of measured deviation angles were gradually increased and saturated as the line width increased. When the line widths were smaller than the lengths of the Si NWs ( $\leq 10 \mu\text{m}$ ), most of the Si NWs were aligned with respect to the direction of the line-patterned structure. On the contrary, when the line widths were larger than the lengths of the Si NWs ( $\geq 10 \mu\text{m}$ ), the Si NWs were not efficiently aligned along the direction of the line patterns since the assembled NWs in the trenches could be rotated during the evaporation of the solvent. Notably, the assembly selectivity of the NWs in polar solution were not affected by the variation of the line widths of the micro-engraved structures.

To better understand the assembly process of NW arrays on micro-engraved substrates during evaporation of the NW solution, we using an in-situ optical microscope to monitor the evaporation procedure. The movements of NWs in polar NW solution (DI water) as a function of time are shown in **Figure 3a–d**. During the evaporation process, the dispersed NWs moved actively because of the internal flow of the solvent (**Figure 3a,b**), and the NW sedimentations located near the micro-engraved patterns were gradually driven into the structures (**Figure 3c,d**). In contrast, much more restricted movement of the NWs was observed in nonpolar solutions. Hence, in polar solutions, there is a much higher probability that NWs will assemble in grooves because of the active movement of NWs near the surface of the sample.

The different activities of NWs inside solutions according to the polarity of the solvent can be explained by the internal hydrodynamic flow during the solvent evaporation step, as

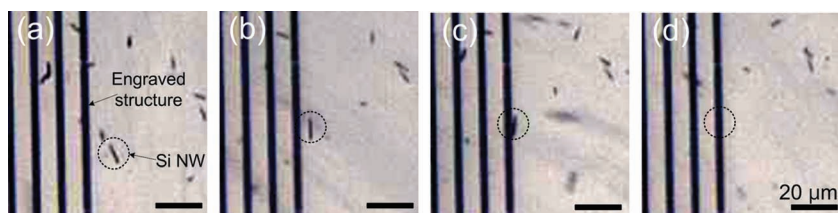


**Figure 3.** Optical microscope images showing the movement of NWs near line-patterned micro-engraved structures due to the internal flow of solvent as a function of time. The NW moves toward the micro-engraved structures (a,b) and is captured at the micro-grooves with aligned directions (c,d). The scale bars in the images indicate 20  $\mu\text{m}$ .

depicted in **Figure 4**. Evaporation modes are determined by various factors, such as the polarity of the solvent and substrate surface, the geometrical properties of the surface, and the evaporation rate of the solvent. Two modes are distinguishable during the evaporation of a droplet from a flat, solid surface: in the first mode, the contact area of the solvent–substrate remains constant while the contact angle decreases during evaporation, which is known as the *pinned* contact mode; in the second mode, the contact angle remains constant and the contact area decreases as evaporation proceeds, which is known as the *depinned* contact mode. In reality, evaporation is governed by either one of these two modes, or a third mode that is a combination of the first two

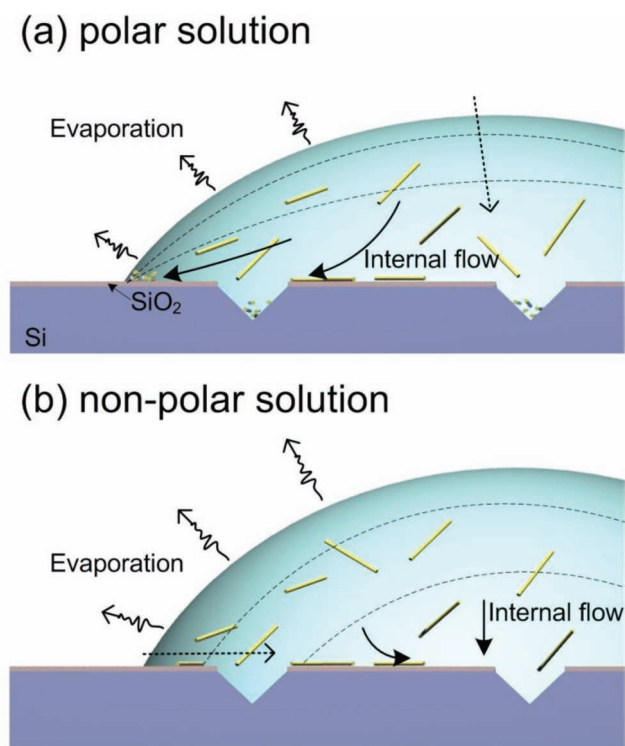


**Figure 4.** Schematic representations of the internal hydrodynamic flow in a NW solution during solvent evaporation. In both figures, the dotted curves represent the free surfaces of the NW solution droplets as evaporation proceeds. a) Schematic of hydrodynamic flow in a polar solution with a *pinned* contact line. b) Schematic of hydrodynamic flow in a nonpolar solution with a *depinned* contact line.

modes. Specifically, in combination mode, evaporation begins in the *pinned* mode and is followed by the *depinned* mode: the contact line of the droplet during the evaporation is ‘stick’ (*pinned* contact mode) until the contact angle decreases to a critical value known as the receding contact-angle limit, and is then superseded by the *depinned* contact mode.<sup>[36,37]</sup>

During our evaporation experiments, we observed that the active motions of the NWs and their assembly into the micro-engraved structures occurred mostly

during the *pinned* contact mode in *hydrophilic* solutions. In the *pinned* contact mode, as the droplet evaporates, the free surface of the liquid moves downward with decreasing contact angle (depicted as dotted lines in Figure 4a), and a hydrodynamic flow-field is generated in the solvent toward the periphery to compensate for the loss of solvent near the contact line. Consequently, the induced flow toward the contact line causes the active motion of suspended NWs. These actively moving NWs can be captured efficiently by the micro-engraved structures, as shown in Figure 4a. In contrast, during the evaporation of nonpolar solvents, the *depinned* contact mode is dominant. The free surface of droplets containing NWs shrinks with a constant contact angle, and a hydrodynamic flow field is engendered toward the center of the contact area between the droplet and surface, as shown in Figure 4b. However, its local velocity is much smaller than that of the hydrodynamic flow field induced by the *pinned* contact mode.<sup>[38]</sup> In addition, the relatively low surface tension and fast evaporation rate of nonpolar solvents could constrain the free motion of suspended NWs, resulting in randomly-oriented NWs after complete evaporation of nonpolar NW solution. Similar polarity dependency as that observed in our NW alignment procedure has been reported previously for various nanoparticles such as carbon nanotubes, polymer latex, and silica nanoparticles.<sup>[39–41]</sup>

However, the increased internal hydrodynamic flow in the *pinned* contact mode cannot fully explain the high selectivity (~95%) of assembly of the NWs, because the internal flow of solvent should also enhance the rate of NW release from the micro-engraved structures to bulk solution during the evaporation process. To determine the assembly characteristics of Si NWs in the micro-engraved structures, we performed the NW aligning process using a large truncated pyramid structure with dimensions of 150  $\mu\text{m} \times 150 \mu\text{m}$ . As shown in **Figure 5a**, the NWs used in our experiment varied in size; NWs with relatively large diameters first nucleated parallel to the edges of the square, followed by the deposition of smaller NWs along the flat surface. A typical top-view of aligned Si NWs in a micro-engraved structure is provided in Figure 5b, demonstrating the highly ordered, close-packed Si NW array structure obtained. Based on the results shown in Figure 5a, we predicted that Si NW assembly in micro-engraved structures would have similar nucleation and deposition characteristics to Si NW assembly in the larger truncated pyramid structure. Figure 5c shows a cross-sectional image of an assembled NW array, taken along the line A–A’ shown in Figure 5b. As

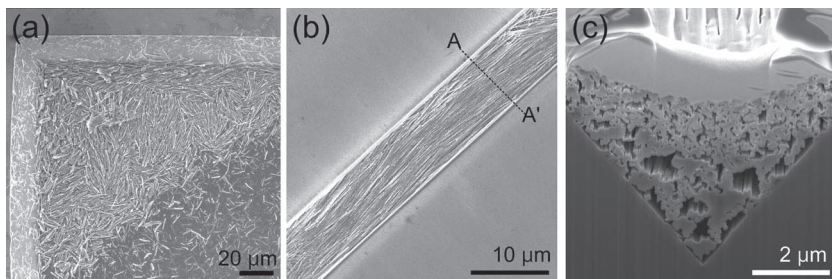


**Figure 5.** a) SEM images of assembled NW arrays in a truncated pyramid structure with dimensions of 150 μm × 150 μm. b) SEM image of a highly aligned NW array at the micro-engraved structure. c) Cross-sectional view of the aligned Si NW array at the micro-engraved structure, which was investigated using a dual beam focused ion beam system.

expected, the sequential deposition of NWs was dominant during the assembly of the NW array. During the early stages of assembly, large NWs were nucleated along the edges of the engraved structure. Subsequently, small NWs driven into the engraved-channel were self-assembled adjacent to the nucleated large NWs, resulting in stacking along the micro-engraved structures.

Such size-dependent sequential NW deposition in a pre-defined structure can be explained by the entropic “depletion attraction” between NWs and the corners of micro-engraved structures.<sup>[42]</sup> A schematic illustration of depletion attraction in colloidal solution containing two differently-sized particles (a small particle with a length of  $L_s$  and a large particle with a radius of  $a$  and a length of  $L_L$ ) is provided in **Figure 6a**. In the colloidal solution containing nanoparticles of different sizes, each particle has an excluded volume equal to the sum of the particle volume and the depletion zone. The depletion zone is a virtual shell surrounding each particle where the centers of small particles cannot be accessible. The width

of the depletion zone is indicated by  $\Delta$  in **Figure 6a**. When large particles are in close proximity, a region of overlap between the two large particles develops; this increases the volume available for small particles, resulting in a decrease in the total free energy of the system. Thus, it results in depletion attraction between large particles, acting to push large particles together. The decrease in the free energy of the system can be defined as  $F = -k_B T \ln Z$ , where  $k_B$  is the Boltzmann constant,  $T$  is the temperature, and  $Z$  is a canonical partition function. In the case of a dilute solution, the canonical partition function is well approximated as  $Z = \{V_0 + V_{ex}(x)\}N$ , where  $N$  is the total number of solute particles,  $V_0$  is the initial volume of solution, and  $V_{ex}$  is the overlap region gained as a function of the distance between large particles (denoted as  $x$  in **Figure 6a**). Thus, we can derive the free energy difference of the system when two large particles are aggregated or separated as follows:

$$\Delta F(x) = F(x) - F(\infty) = -Nk_B T \ln \left[ 1 + \frac{V_{ex}(x)}{V_0} \right] \quad (1)$$

Based upon Equation (1), the difference in free energy is relevant to both the concentration of the solution and the geometric factors of the particles. Specifically, it is clear that NWs experience significantly enhanced depletion attraction compared to spherically shaped nanoparticles even for very small volume fractions of solute NWs, because the restriction in rotational degrees of freedom of small NWs can induce depletion forces. Furthermore,

when large NWs are in parallel contact, the volume of the overlap region generated is much larger than that created by spherically-shaped particles.<sup>[43,44]</sup> This attraction force can explain the interaction between particles and the walls of the micro-structures. An illustration of the overlapped excluded volume when a large NW approaches the corner or notch of a pre-defined structure with an inward slope of  $\theta$  is shown in **Figure 6b**. It can be intuitively inferred that the agglomeration of NWs is thermodynamically more stable than their separation, because the attraction force is a function of the volume of the overlap region that develops. Similarly, deposition of NWs in the corners of the micro-engraved structures is expected to be more energetically favorable than agglomeration of NWs in solution.

Due to the high complexity of the actual movements of the NWs in solution, it is not easy to examine the interactions

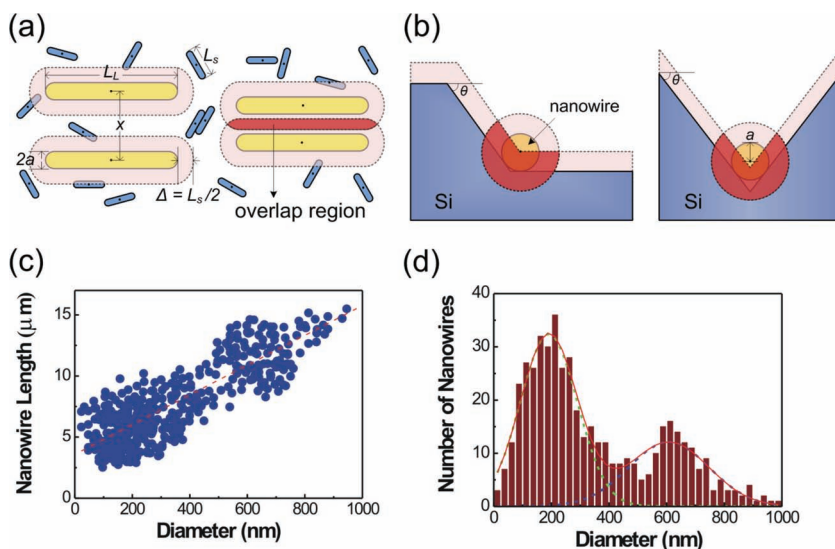


**Figure 6.** a) Schematic illustration of depletion attraction in the NW solution. b) Illustration of the overlapped regions that developed when NWs were located at the corner of the truncated pyramid structure (left) and micro-engraved structure (right). c) The distributions of the diameters and lengths of the NWs in solution. The dotted line is a linear fitting curve. d) Histogram of the diameter distribution of NWs. These results clearly show that NWs can be classified into two groups according to their size.

of NWs in solution. To develop a thermodynamic model for our system, we made the following assumptions: NWs are cylindrically shaped; the NW solution is continuum dispersed; NWs experience a hard-core interaction. The volume of the overlapping region between a NW and a V-shaped engraved structure when the NW is located at the notch tip can be calculated as follows (see the SI, Modeling and Calculations):

$$V_{ex} = \begin{cases} \left[ \begin{aligned} & \left[ (a + \Delta)^2 \left\{ \theta + \cos^{-1} \left( \frac{a - \Delta}{a + \Delta} \right) \right\} \right. \\ & \left. - \frac{(a + \Delta)(a - \Delta)}{\cos \theta} \right. \\ & \left. \times \sin \left\{ \theta + \cos^{-1} \left( \frac{a - \Delta}{a + \Delta} \right) \right\} \right] \cdot L_L, \\ & \text{where } 0 < \Delta < a \left( \frac{1 + \cos \theta}{1 - \cos \theta} \right), \\ & \pi (a + \Delta)^2 \cdot L_L, \\ & \text{where } \Delta > a \left( \frac{1 + \cos \theta}{1 - \cos \theta} \right) \end{aligned} \right] \end{cases} \quad (2)$$

To determine the geometric characteristics of NWs suspended in a solution, careful SEM analyses were carried out. Figure 6c shows the diameter and length distributions of the NWs in solution. The length of NWs was linearly related to the diameter of NWs. This characteristic may be due to the sonication process used to prepare the NW solution, because NWs with smaller diameters can more easily be broken than those with larger diameters. The NWs ranged in diameter from 25 to 940 nm, and in length from 2.5 to 15  $\mu\text{m}$ . The diameter distribution of the NWs analyzed in Figure 6c is shown in Figure 6d. Two distinct peaks were evident in the histogram, indicating that the NWs in solution could be categorized into two groups: smaller-sized NWs and larger-sized NWs with an average diameter and length of 190 nm/5.5  $\mu\text{m}$  and 600 nm/9  $\mu\text{m}$ , respectively. Assuming binary dispersion, we calculated the decreased free energy ( $\Delta F$ ) of the system for the case when a NW is located near the tip of a notch using Equation (1) and (2): when a large NW nucleated,  $\Delta F$  was  $-8.6k_B T$ . The magnitude of this interaction is much larger than the thermal energy,  $k_B T$ . Consequently, it is more energetically favorable for NWs to be confined at the corner of the micro-engraved structure than for them to diffuse out into the bulk solution, which explains the observed nucleation and deposition of NWs in the engraved structures during evaporation.

We fabricated back-gated flexible FETs to investigate the feasibility of our proposed direct gravure printing method. As illustrated in Figure 7a, the aligned NW arrays were transferred onto a flexible

substrate with a back-gate electrode and a gate dielectric layer (PET substrate/100 nm-thick ITO/100 nm-thick  $\text{Al}_2\text{O}_3$ ) using the direct gravure printing method. An SU-8 epoxy layer was used as the bonding layer between the NW arrays and substrate. It is noteworthy that the printed Si NW array patterns consist of a single or bi-layer of Si NW film since only the Si NWs that were directly in contact with the highly adhesive PDMS stamp (located at the top of the assembled nanowire arrays in the micro-engraved structures) could be transferred during the direct gravure printing process. After transfer of the Si NWs, the source and drain electrodes were defined using a tungsten stencil mask. The resulting devices had a channel length of approximately 8  $\mu\text{m}$ . An image of a fabricated NW FET on a bent PET substrate is shown in Figure 7b. The logarithmic-scale transfer characteristics curve of the fabricated Si NW FET device at a fixed drain-source voltage  $V_{DS}$  of 5 V is shown in Figure 7c. The NW transistor showed typical p-type characteristics and the measured on/off ratio was  $\sim 2.6 \times 10^5$  with the subthreshold slope was 500 mV/decade. The transconductance ( $g_m$ ) and turn-on threshold voltage ( $V_{th}$ ), estimated by fitting the linear part of the drain-source current ( $I_{DS}$ )– $V_{GS}$  curve, were 92 nS and 2.1 V, respectively. The effective hole mobility ( $\mu_h$ ) was calculated using the following equation:

$$g_m = \frac{\partial I_{DS}}{\partial V_{DS}} = \frac{\mu_h V_{DS} W c_i}{L} \quad (3)$$

where  $c_i$  is the capacitance per unit area of gate dielectric,  $W$  is the channel width, and  $L$  is the channel length of the FET.

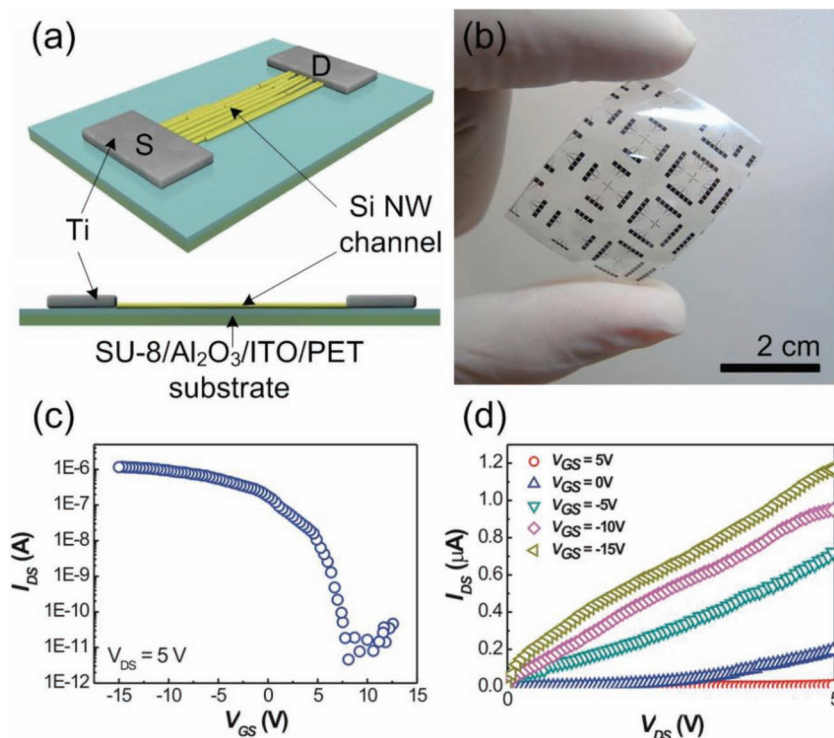


**Figure 7.** Si NW FET on a flexible substrate. a) A schematic showing the device configuration of a back-gated Si NW FET on PET substrate. b) A picture of the flexible device with the Si NW FET device. The scale bar indicates 2 cm. c)  $I_{DS}$ – $V_{GS}$  relationship for the Si NW FET device at  $V_{DS} = 5$  V. d)  $I_{DS}$ – $V_{DS}$  relation at  $V_{GS}$  varying from 5 to  $-15$  V with increasing steps of  $-5$  V.

The corresponding hole mobility ( $\mu_h$ ) was  $17.1 \text{ cm}^2\text{V}^{-1}\text{s}^{-1}$  at  $V_{\text{DS}} = 5 \text{ V}$ . A representative output curve ( $I_{\text{DS}}-V_{\text{DS}}$ ) that was measured by varying the gate bias from 5 to  $-15 \text{ V}$  is shown in Figure 7d. As indicated in the output curve, the drain current of the fabricated transistor increased with respect to the drain voltage, rather than showing a clear saturation regime. This tendency possibly originates from the increased carrier scattering induced by the complex NW network paths, the large surface roughness of the NWs, and the rather poor electrical contacts induced by the residual polymer between the NWs and electrodes.<sup>[45,46]</sup>

### 3. Conclusion

In summary, we developed a novel NW alignment method that exploits the hydrodynamic flow of the solvent and entropic attraction during solvent evaporation; our method therefore does not require any additional applied forces or chemical treatments. We also derived a hydrodynamic flow model of the solvent and entropic force fields during evaporation that was able to explain the well-aligned Si NW arrays that assembled on the micro-engraved structures fairly accurately. As droplets evaporate, the internal hydrodynamic flow of solvent leads to the assembly of NWs on the micro-engraved structures. The internal flow of the solvent is highly dependent on the polarity of the solvent. NWs that encounter micro-engraved structures are spontaneously confined at the corners of the engraved structures, and this behavior is size-dependent; larger-diameter NWs are deposited first followed by smaller ones, due to entropic force fields. The aligned NW arrays can be successfully transferred to flexible substrates using direct gravure printing; we demonstrated this by fabricating and characterizing FETs. Our results have implications for the fabrication of inorganic active component-based printable electronics on mechanically flexible substrates.

### 4. Experimental Section

**Si NW Fabrication and Preparation of NW Solutions:** A (100) oriented p-type Si substrate ( $1-10 \text{ }\Omega\text{-cm}$ ) was successively cleaned with acetone, isopropanol (IPA), and DI water. The native oxide was removed by immersing the substrate into 5% HF aqueous solution for 3 min at room temperature. The cleaned Si substrate was then immediately dipped in a solution containing 30 mM of  $\text{AgNO}_3$  and 4.9 M of HF for 50 min at  $80 \text{ }^\circ\text{C}$ . The undesired by-products (silver dendrites and silver nanoparticles) generated during the NW fabrication removed by successive rinsing the substrate with 30 wt.%  $\text{HNO}_3$  aqueous solution and de-ionized (DI) water. To obtain well-dispersed NW solutions, the fabricated Si NWs were cut into the various polar solutions (IPA, DI water, methyl alcohol, and acetone) and nonpolar solutions (toluene, methylene chloride, and chloroform), followed by sonication for 30 s.

**Fabrication of Micro-engraved Patterned Substrates:** Si substrates with anisotropically etched micro-engraved structures were prepared as follows. A (100)-oriented p-type Si substrate was oxidized under wet conditions at  $1000 \text{ }^\circ\text{C}$  to grow a thick  $\text{SiO}_2$  layer of 700 nm. The substrate covered with the  $\text{SiO}_2$  layer was patterned using photo-lithography followed by a reactive etching process.

Then, the patterned structures were etched anisotropically in 25 wt.% tetramethylammonium hydroxide (TMAH) solution at  $85 \text{ }^\circ\text{C}$ , yielding micro-engraved structures with Si(111) facets with an inward slope angle of  $54.7^\circ$ . During the etching process, IPA was added to the TMAH solution to minimize the undercutting ratio, and the volume ratio of IPA was maintained at approximately 15%.

**Direct Gravure Printing of NW Arrays on Flexible Substrates:** The Si NW solutions were dropped onto micro-engraved patterned substrates with a size of  $20 \text{ mm} \times 20 \text{ mm}$ . After the entire alignment process was completed, the undesired NWs that were not located on the micro-engraved structures were selectively removed by rigid PDMS with low adhesion strength (Sylgard 184 base and curing agent at a volume ratio of 5:1). The density of NWs in the engraved structures could be controlled by repeating the dropping and evaporation steps, and redundant NWs on the substrate were minimized without affecting the shape of the aligned NW arrays in the micro-engraved structures, as shown in Figure S1a (SI). Subsequently, the aligned Si NWs were detached from the microchannels by using a soft PDMS with high adhesive strength (volume ratio of base to curing agent of 10:1). A plastic substrate, namely 150- $\mu\text{m}$ -thick PET coated with a 100-nm-thick ITO film, was used as the receive substrate. A 100-nm-thick  $\text{Al}_2\text{O}_3$  gate dielectric layer was deposited using atomic layer deposition (ALD), followed by spin-coating of the 2- $\mu\text{m}$ -thick epoxy bonding layer (SU-8 2002, Microchem) at 4000 rpm for 60 s. The epoxy-layer-coated substrate was pre-cured on a hot plate at  $90 \text{ }^\circ\text{C}$  for 1 min, and then the PDMS containing the aligned NW arrays was placed on top of the sample in a conformal manner. A subsequent curing process was carried out on a hot plate at  $90 \text{ }^\circ\text{C}$  for 5 min. After the curing process was finalized, the PDMS was carefully peeled off. As shown in Figure S1b (SI), Si NW arrays were successfully transferred onto the flexible substrate after the direct gravure printing process.

**Fabrication of FETs on Flexible Substrate:** A 75-nm-thick Ti electrode layer was thermally evaporated on the flexible substrate containing the aligned NW arrays as an electrode. The source and drain electrodes were defined by a tungsten wire stencil with a diameter of  $8 \text{ }\mu\text{m}$  in Si NW FETs.

**Characterization:** The movements of NWs in the solutions during the evaporation step were examined more closely by using an in-situ optical microscope with a mounted digital camera (ARTCAM 300MI). Aligned NW network arrays were observed with a JEOL JSM-6360 field emission scanning electron microscope (FE-SEM). To investigate cross-sections of aligned NW arrays, focused ion beam (FIB) analysis was carried out using the dual beam FIB system (NOVA600 NANOLAB). The  $\text{Ga}^+$  ion beam was tilted  $52^\circ$  with respect to the electron beam. The aligned NW network arrays were roughly milled with a  $\text{Ga}^+$  ion beam (typically, a beam current of  $\sim 3 \text{ nA}$  and an acceleration voltage of  $30 \text{ keV}$ ). The milled surface was then polished with a low beam current ( $\sim 500 \text{ pA}$ ) followed by SEM imaging. The electrical properties of NW FETs were characterized by using a Keithley 236 source measurement unit (SMU).

### Supporting Information

Supporting Information is available from the Wiley Online Library or from the author.

## Acknowledgements

This research was partially supported by the Converging Research Center Program through the Ministry of Education, Science, and Technology (No. 2011K000631) and by the Priority Research Centers Program through the National Research Foundation of Korea (NRF) funded by the Ministry of Education, Science and Technology (2009-0093823). This work was also supported by the KARI-University Partnership program and a National Research Foundation of Korea (NRF) grant funded by the Korean government (MEST) (No. 2011-0028594). T.I. Lee and J.M. Myoung were supported by WCU(World Class University) program through the National Research Foundation of Korea funded by the Ministry of Education, Science, and Technology (R32-20031).

- [1] G. Zheng, W. Lu, S. Jin, C. M. Lieber, *Adv. Mater.* **2004**, *16*, 1890.
- [2] Y. Cui, Z. Zhong, D. Wang, W. U. Wang, C. M. Lieber, *Nano Lett.* **2003**, *3*, 149.
- [3] Y. Huang, X. Duan, Y. Cui, C. M. Lieber, *Nano Lett.* **2002**, *2*, 101.
- [4] X. Duan, Y. Huang, R. Agarwal, C. M. Lieber, *Nature* **2003**, *421*, 241.
- [5] M. S. Gudiksen, L. J. Lauhon, J. Wang, D. C. Smith, C. M. Lieber, *Nature* **2002**, *415*, 617.
- [6] J. Xiang, W. Lu, Y. Hu, Y. Wu, H. Yan, C. M. Lieber, *Nature* **2006**, *441*, 489.
- [7] Y. Cui, Q. Wei, H. Park, C. M. Lieber, *Science* **2001**, *293*, 1289.
- [8] R. S. Friedman, M. C. McAlpine, D. S. Ricketts, D. Ham, C. M. Lieber, *Nature* **2005**, *434*, 1085.
- [9] Y. Huang, X. Duan, Y. Cui, L. J. Lauhon, K. H. Kim, C. M. Lieber, *Science* **2001**, *294*, 1313.
- [10] A. Javey, J. Guo, Q. Wang, M. Lundstrom, H. Dai, *Nature* **2003**, *424*, 654.
- [11] J. Kong, N. R. Franklin, C. Zhou, M. G. Chapline, S. Peng, K. Cho, H. Dai, *Science* **2000**, *287*, 622.
- [12] M. E. Roberts, M. C. Lemieux, Z. Bao, *ACS Nano* **2009**, *3*, 3287.
- [13] S. Hong, S. Myung, *Nat. Nanotechnol.* **2007**, *2*, 207.
- [14] W. Lu, C. M. Lieber, *Nat. Mater.* **2007**, *6*, 841.
- [15] F. Xu, W. Lu, Y. Zhu, *ACS Nano* **2011**, *5*, 672.
- [16] Y. Sun, J. A. Rogers, *Nano Lett.* **2004**, *4*, 1953.
- [17] M. C. McAlpine, H. Ahmad, D. Wang, J. R. Heath, *Nat. Mater.* **2007**, *6*, 379.
- [18] A. J. Baca, J. H. Ahn, Y. Sun, M. A. Meitl, E. Menard, H. S. Kim, W. M. Choi, D. H. Kim, Y. Huang, J. A. Rogers, *Angew. Chem. Int. Ed.* **2008**, *47*, 5524.
- [19] D. Whang, S. Jin, Y. Wu, C. M. Lieber, *Nano Lett.* **2003**, *3*, 1255.
- [20] P. Smith, C. Nordquist, T. Jackson, T. Mayer, B. Martin, J. Mbindyo, T. Mallouk, *Appl. Phys. Lett.* **2000**, *77*, 1399.
- [21] O. Harnack, C. Pacholski, H. Weller, A. Yasuda, J. M. Wessels, *Nano Lett.* **2003**, *3*, 1097.
- [22] W. Salalha, E. Zussman, *Phys. Fluids* **2005**, *17*, 063301.
- [23] Y. Huang, X. Duan, Q. Wei, C. M. Lieber, *Science* **2001**, *291*, 630.
- [24] B. Sun, H. Siringhaus, *J. Am. Chem. Soc.* **2006**, *128*, 16231.
- [25] Y. Cui, M. T. Björk, J. A. Liddle, C. Sönnichsen, B. Boussert, A. P. Alivisatos, *Nano Lett.* **2004**, *4*, 1093.
- [26] Y. Yin, Y. Lu, B. Gates, Y. Xia, *J. Am. Chem. Soc.* **2001**, *123*, 8718.
- [27] M. Engel, J. P. Small, M. Steiner, M. Freitag, A. A. Green, M. C. Hersam, P. Avouris, *ACS Nano* **2008**, *2*, 2445.
- [28] G. Yu, A. Cao, C. M. Lieber, *Nat. Nano* **2007**, *2*, 372.
- [29] K. Heo, E. Cho, J. E. Yang, M. H. Kim, M. Lee, B. Y. Lee, S. G. Kwon, M. S. Lee, M. H. Jo, H. J. Choi, *Nano Lett.* **2008**, *8*, 4523.
- [30] S. G. Rao, L. Huang, W. Setyawan, S. Hong, *Nature* **2003**, *425*, 36.
- [31] A. Javey, S. Nam, R. S. Friedman, H. Yan, C. M. Lieber, *Nano Lett.* **2007**, *7*, 773.
- [32] R. D. Deegan, O. Bakajin, T. F. Dupont, G. Huber, S. R. Nagel, T. A. Witten, *Nature* **1997**, *389*, 827.
- [33] J. Huang, R. Fan, S. Connor, P. Yang, *Angew. Chem. Int. Ed.* **2007**, *46*, 2414.
- [34] Y. Li, Y. Wu, *J. Am. Chem. Soc.* **2009**, *131*, 5851.
- [35] K. Peng, A. Lu, R. Zhang, S. Lee, *Adv. Funct. Mater.* **2008**, *18*, 3026.
- [36] R. G. Picknett, R. Bexon, *J. Colloid Interface Sci.* **1977**, *61*, 336.
- [37] H. Z. Yu, D. M. Soolaman, A. W. Rowe, J. T. Banks, *ChemPhysChem.* **2004**, *5*, 1035.
- [38] A. J. Petsi, V. N. Burganos, *Phys. Rev. E: Stat., Nonlinear, Soft Matter Phys.* **2008**, *78*.
- [39] K. Uno, K. Hayashi, T. Hayashi, K. Ito, H. Kitano, *Colloid Polym. Sci.* **1998**, *276*, 810.
- [40] H. Y. Ko, J. Park, H. Shin, J. Moon, *Chem. Mater.* **2004**, *16*, 4212.
- [41] A. Amma, B. Razavi, S. K. St. Angela, T. S. Mayer, T. E. Mallouk, *Adv. Funct. Mater.* **2003**, *13*, 365.
- [42] S. Asakura, F. Oosawa, *J. Chem. Phys.* **1954**, *22*, 1255.
- [43] K. J. M. Bishop, C. E. Wilmer, S. Soh, B. A. Grzybowski, *Small* **2009**, *5*, 1600.
- [44] K. A. Smith, S. Tyagi, A. C. Balazs, *Macromolecules* **2005**, *38*, 10138.
- [45] J. H. Choi, J. P. Kar, D. Y. Khang, J. M. Myoung, *J. Phys. Chem.* **2009**, *113*, 5010.
- [46] G. D. Yuan, Y. B. Zhou, C. S. Guo, W. J. Zhang, Y. B. Tang, Y. Q. Li, Z. H. Chen, Z. B. He, X. J. Zhang, P. F. Wang, *ACS Nano* **2010**, *4*, 3045.

Received: January 13, 2012  
 Published online: March 19, 2012